Bulletin of the Seismological Society of America, 91, 3, pp. 617–623, June 2001

Short Notes

Accuracy of the Explicit Planar Free-Surface Boundary Condition Implemented in a Fourth-Order Staggered-Grid Velocity-Stress Finite-Difference Scheme

by E. Gottschämmer and K. B. Olsen

Abstract We compute the accuracy of two implementations of the explicit planar free-surface boundary condition for 3D fourth-order velocity-stress staggered-grid finite differences, 1/2 grid apart vertically, in a uniform half-space. Due to the staggered grid, the closest distance between the free surface and some wave-field components for both implementations is 1/2-grid spacing. Overall, the differences in accuracy of the two implementations are small. When compared to a reflectivity solution computed at the staggered positions closest to the surface, the total misfit for all three components of the wave field is generally found to be larger for the free surface colocated with the normal stresses, compared to that for the free surface colocated with the *xz* and *yz* stresses. However, this trend is reversed when compared to the reflectivity solution exactly at the free surface (the misfit encountered in staggered-grid modeling). When the wave field is averaged across the free surface, thereby centering the staggered wave field exactly on the free surface, the free-surface condition colocated with the *xz* and *yz* stresses generates the smallest total misfit for increasing epicentral distance. For an epicentral distance/hypocentral depth of 10, the total misfit of this condition is about 15% smaller than that for the condition colocated with the normal stresses, mainly controlled by the misfit on the Rayleigh wave.

Introduction

The numerical treatment of the free surface in finite-difference (FD) methods has received considerable attention in the literature. The majority of these publications concern the treatment of irregular free surfaces, in order to simulate the effects of topographic scattering (e.g., Robertsson, 1996; Ohminato and Chouet, 1997; Hestholm and Ruud, 1998). However, while these methods allow the flexibility of including mountain topography, they also generally require a relative dense sampling of the wave field for accurate results. For example, Ohminato and Chouet (1997) find that 25 points per wavelength are required for stable and accurate results using their irregular free surface. In the cases where effects of surface relief are expected to be negligible, namely, for long-period waves propagating in areas of smooth topography, it is possible to formulate an explicit boundary condition valid for a planar surface (e.g., Graves, 1996; Levander, 1988). The advantage of these formulations are generally that they require less points per wavelengths compared with those for irregular free-surface boundary conditions, namely, the explicit planar condition by Levander (1988) that is accurate for only 5 points per wavelength. Clearly, the explicit free-surface condition should be considered for numerical reasons in situations where applicable.

The velocity-stress staggered-grid FD method, in particular the 3D 2–4 implementation (second-order accurate in time and fourth-order accurate in space) has become increasingly popular for simulating ground motion, both for kinematic (e.g., Olsen, 1994; Olsen *et al.,* 1995; Olsen and Archuleta, 1996; Graves, 1998; Wald and Graves, 1998; Olsen, 2000; Olsen *et al.,* 2000) and dynamic (e.g., Olsen *et al.,* 1997; Peyrat *et al.,* 2001) methods. These studies all used an explicit, planar free-surface boundary condition, which was found superior in accuracy compared to the vacuum formulation (e.g., Graves, 1996). The explicit planar free-surface condition typically requires two (nonphysical) grid planes above the free surface (Graves, 1996).

There are two different possibilities for the implementation of the explicit free-surface boundary condition in the staggered grid, 1/2 grid points apart vertically. Graves (1996) described the implementation colocated with the nor-

mal stress positions, hereafter denoted FS1. It is also possible to implement the free surface colocated with the *xz* and *yz* stresses, offset 1/2 grid vertically from the Graves (1996) implementation (hereafter denoted FS2). While the ground motion and rupture dynamics simulations listed above include both implementations of the free-surface boundary condition, differences in accuracy have to our knowledge not been documented.

This study contains an analysis of the relative accuracy of the planar free-surface boundary conditions FS1 and FS2. The main incentive for our study is a preliminary test that we carried out in the Southern California Earthquake Center (SCEC) 3D velocity model, showing significant differences between long-period ground-motion synthetics computed using the two different boundary conditions for planar free surfaces, in particular for sediment sites. These differences were comparable to the error expected from unaccounted topographic effects due to the use of a planar free surface. Lacking an analytical solution for the heterogeneous model, we attempted to validate the synthetics against strong-motion data. Unfortunately, due to the resolution of the model and an artificially imposed minimum velocity due to computational limitations, the fit of the synthetics to the data were not significantly improved by either free-surface condition. However, the result demonstrated that the choice of the two free-surface boundary conditions makes a difference for a realistic earth model.

Part of the discrepancy between the exact ground motion at the free surface and that for the explicit free-surface boundary conditions is due to the positioning of some components of the wave field 1/2 grid points below the surface for the staggered grids. It is not obvious to what extent, if any, the wave field at the two grid planes above the free surface can be used to minimize the misfit due to the location of some components 1/2 grid points below the free surface. In this article, we investigate the possibility of averaging the wave field across the free surface in order to increase the accuracy of the numerical solution at the free surface.

Explicit Free-Surface Boundary Condition

We use a fourth-order staggered-grid FD scheme to solve the 3D elastic equations of motion (Olsen, 1994; Graves, 1996) (Fig. 1). The absorbing boundaries were moved far enough away to avoid any artificial reflections.

The source is implemented in the FD grid by adding

$$-\Delta t \dot{M}_{ij}(t)/V \tag{1}$$

to $\sigma_{ij}(t)$ where $\dot{M}_{ij}(t)$ is the *ij*th component of the moment rate tensor for the earthquake, $V = dx^3$ is the cell volume, and $\sigma_{ij}(t)$ is the *ij*th component of the stress tensor on the fault at time *t* (Olsen *et al.,* 1995).

At the free surface, we must satisfy

$$\tau_{zz} = \tau_{xz} = \tau_{yz} = 0. \tag{2}$$

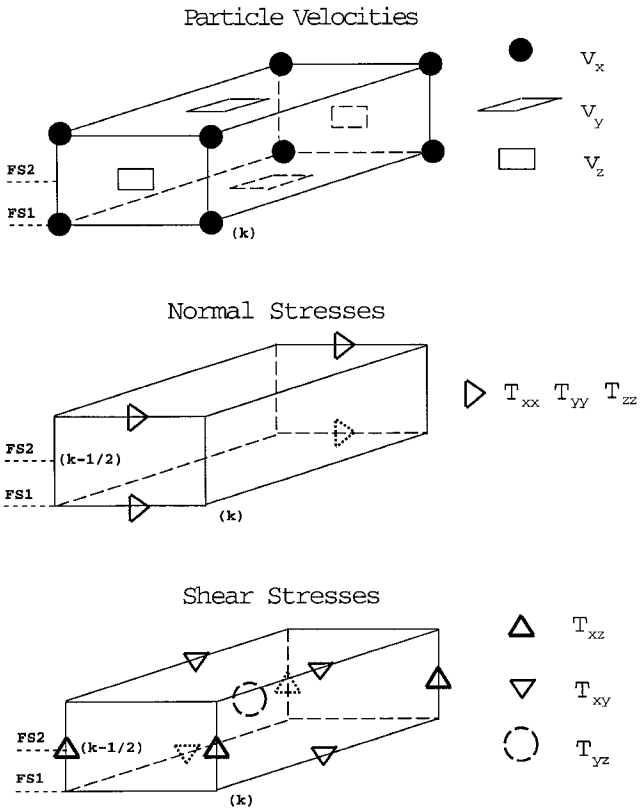

Figure 1. Staggering of the wave field parameters.

We examine the accuracy of the explicit, planar free-surface boundary condition colocated with the normal stresses (τ_{xx}, τ_{yy}, τ_{zz}) (FS1) and that colocated with the shear stresses τ_{xz} and τ_{yz} (FS2) (see Fig. 1). For implementation FS1, the horizontal velocities v_x and v_y are located exactly at the free surface, while the vertical velocity v_z is located 1/2 grid point below. For implementation FS2, the horizontal velocities v_x and v_y are positioned 1/2 grid point below the free surface, while the vertical velocity v_z is located exactly at the surface. Our coordinate system is right handed, with the *z* axis positive downward.

Free-Surface Boundary Condition FS1

Implementation FS1 was described by Graves (1996). His equations (15) and (16) are summarized in this section. Let the free surface be located at vertical index *k*. τ_{zz} is located at the surface and is explicitly set to zero:

$$\tau_{zz}^{k} = 0. \tag{3}$$

τ_{zz}, τ_{xz}, and τ_{yz} above the free surface are obtained using antisymmetry:

$$\tau_{zz}^{k-1} = -\tau_{zz}^{k+1},$$

$$\tau_{xz}^{k-1/2} = -\tau_{xz}^{k+1/2},\ \tau_{xz}^{k-3/2} = -\tau_{xz}^{k+3/2},$$
$$\tau_{yz}^{k-1/2} = -\tau_{yz}^{k+1/2}, \text{ and } \tau_{yz}^{k-3/2} = -\tau_{yz}^{k+3/2}. \quad (4)$$

τ_{xx}, τ_{yy}, and τ_{xy} are not used above the free surface. Using equations (2) and (3), we can derive the following difference equations for the velocity at and above the free surface:

$$D_z v_z^k = \frac{-\lambda}{\lambda + 2\mu}[D_x v_x^k + D_y v_y^k]$$
$$[D_z v_x + D_x v_z]^{k-1/2} = -[D_z v_x + D_x v_z]^{k+1/2}$$
$$[D_z v_y + D_y v_z]^{k-1/2} = -[D_z v_y + D_y v_z]^{k+1/2} \quad (5)$$

where D_l^n represents a centered, second-order approximation to the differential operator $\partial/\partial l$ in direction l direction at vertical level n.

For implementation FS1, special attention must be given to the computation of the horizontal normal stresses (τ_{xx} and τ_{yy}) at the surface, because they involve the vertical velocity at 3/2 grid points above the surface. This value is usually not solved by the previous second-order difference equations (Graves, 1996). The most obvious choice is to use second-order accuracy in the computation of the vertical derivatives of the horizontal normal stresses at the free surface for FS1, which is the implementation that we will discuss subsequently. We also tested the accuracy of using fourth-order accuracy and simply setting $v_z = 0$ at 3/2 grid points above the surface. However, the accuracy of the latter implementation was worse than the former everywhere.

Free-Surface Boundary Condition FS2

Implementation FS2 is defined by locating the surface at $k - 1/2$, namely, 1/2 grid point vertically apart from implementation FS1:

$$\tau_{xz}^{k-1/2} = \tau_{yz}^{k-1/2} = 0. \quad (6)$$

τ_{zz}, τ_{xz}, and τ_{yz} above the free surface are obtained using antisymmetry:

$$\tau_{zz}^{k-1} = -\tau_{zz}^{k}$$
$$\tau_{xz}^{k-3/2} = -\tau_{xz}^{k+1/2} \quad (7)$$
$$\tau_{yz}^{k-3/2} = -\tau_{yz}^{k+1/2}.$$

Again, τ_{xx}, τ_{yy}, and τ_{xy} are not used above the free surface. Using equations (5) and (6) we can derive the following difference equations for the velocity at and above the free surface:

$$(\lambda + 2\mu)[D_z v_z]^{k-1} + \lambda[D_y v_y + D_x v_x]^{k-1} =$$
$$-(\lambda + 2\mu)[D_z v_z]^{k} + \lambda[D_y v_y + D_x v_x]^{k}$$
$$D_z v_x^{k-1/2} = -D_x v_z^{k-1/2} \quad (8)$$
$$D_z v_y^{k-1/2} = -D_y v_z^{k-1/2}.$$

Accuracy Tests

Source and Receiver Configuration and Model Description

We used a double-couple point source with a rise time of 0.1 sec inserted at (0 m, 0 m, 2000 m) in a uniform half-space model, with a compressional wave speed of 6.0 km/sec, a shear-wave speed of 3.464 km/sec and a density of 2.7 g/m^3. The only nonzero moment tensor component was M_{xy} (equal to M_{yx}), which had the value $M_0 = 10^{18}$ N m. The moment $M(t)$ and moment rate $\dot{M}(t)$ time histories were

$$M(t) = M_0 \cdot \left(1 - \left(1 + \frac{t}{T}\right) \cdot e^{-t/T}\right) \quad (9)$$

and

$$\dot{M}(t) = M_0 \cdot \left(\frac{t}{T^2}\right) \cdot e^{-t/T}, \quad (10)$$

respectively, where t is time and T is the rise time. For FS1, the source is naturally located at 2 km depth, while for FS2 we approximated the source by the average between xy (0 m, 0 m, 2050 m) and xy (0 m, 0 m, 1950 m). We computed the synthetic velocity time histories at the surface point (i·600 m, 1·800 m, 0 m), i = 1 . . . , 20, namely; the receivers are located along a line oriented at angle 53.13° (i.e., $\tan^{-1}$ (4/3)) to the x axis. We deconvolve the source–time function from the ground-motion time histories and convolve with a Gaussian-shaped function corresponding to approximately 6 points per shear wavelength with $V_s = 3.464$ km/sec and $dx = 100$ m. No attenuation was included in the simulations. The modeling parameters are summarized in Table 1.

Table 1
Modeling Parameters

Spatial discretization (m)	100
Temporal discretization (sec)	0.0075
Number of E–W grid points	750
Number of N–S grid points	750
Number of vertical grid points	297
Number of timesteps	1112
Simulation time (sec)	8.34

Numerical Results

Two sets of comparisons are of relevance in order to measure the accuracy of the FD free-surface boundary conditions. The first is to address the true misfit of the conditions, where the FD solutions are compared to reflectivity solutions computed at the positions of the staggered wavefield components. These positions are 1/2 grid point below the actual free surface for some components because of the staggered grid. The other is to measure the actual misfit, where the FD solutions are always compared to the reflectivity solutions at the free-surface position. The actual misfit is what is generally encountered in reality and includes the true misfit and the misfit introduced by the fact that some parameters are located 1/2 grid point below the surface. We use the method of Bouchon (1981) to compute the reflectivity solution.

Figure 2 shows the misfit of the velocity time histories (SCH) for the two FD free-surface boundary conditions compared to the reflectivity solution. The misfit is measured as

$$\frac{\sqrt{\sum_t \left(S(t)_{\mathrm{REFL}} - S(t)_{\mathrm{FD}}\right)^2}}{\sqrt{\sum_t S(t)^2_{\mathrm{REFL}}}} \tag{11}$$

for the radial, transverse, and vertical components, and for the three components combined. The true misfit is shown in the left column of Figure 2. The misfit is similar and small for the transverse component (<0.03 at an epicentral distance divided by the hypocentral depth [EDHD] of 10), while the appearance of the Rayleigh wave causes that for the radial (32%) and vertical (20%) components as well as the total misfit (22%) here to be smaller for FS2 compared to that for FS1.

The actual misfit is shown in the middle column of Figure 2. At 10 EDHD, FS1 (misfit < 0.15) is superior to FS2 (misfit < 0.1) for the horizontal components (located at the surface for FS1, 1/2 grid point below for FS2), while FS2 (misfit 0.093) is more accurate than FS1 (misfit 0.12) for the vertical component (positioned at the surface for FS2, 1/2 grid point below for FS1). The misfit for FS2 is much larger than that for FS1 close to the epicenter. FS1 is generally more accurate than FS2 when all components are considered.

Figure 3 shows comparisons of the reflectivity solution to the FD solutions and the misfit for the two implementations of the free-surface boundary condition. The residuals are enhanced by a factor of 5 for site 1 for clarity, while the actual residuals are displayed for site 20. The largest (actual) misfit at site 1 (<0.1, see Fig. 2) appears on the horizontal components for FS2. Figure 3 reveals that this misfit is mainly due to a slightly early arrival of the *P* and *S* waves. This timing misfit is in part due to the necessity of averaging the source across grid lines between 1950 and 2050 m, which transfers energy toward earlier (and later) times. However, the fact that the horizontal components here are positioned 1/2 grid point below the surface is by far the largest reason for the slightly early arrival for the FS2 horizontal motions at site 1. The vertical component for FS2 is positioned at the free surface and shows a much smaller misfit. At site 20, by far the largest part of the total misfit is due to the Rayleigh wave (about 0.27 actual misfit for FS2). The largest misfit is indeed expected to be related to the surface waves, which are generated at and propagating close to the free surface. While FS2 is overall more accurate than FS1 (0.18 versus 0.24 true misfit) the staggered positions increase the actual misfit for FS2 at site 20.

As mentioned previously, FS1 requires the use of second-order accuracy in the computation of the vertical derivatives of the horizontal normal stresses at the free surface. Here, we find no significant improvement in the error, whether second-order or fourth-order accuracy is used for the horizontal derivatives of these parameters.

Refinement of FS1 and FS2

Finally, we attempt to improve the accuracy of the two boundary conditions compared to the actual misfit. The obvious suggestion is to average the components that are positioned 1/2 grid point below the free surface with those located 1/2 grid point above the free surface. However, the validity of this procedure is not clear because it involves nonphysical parameters positioned virtually above the surface. On the other hand, the conditions for FS1 and FS2, equations (6) to (8), imply symmetry of the particle velocities across the free surface. The misfit of the averaged parameters is shown in the right column of Figure 2. We obtain a misfit up to three times smaller for the averaged seismograms compared to those at locations 1/2 grid point below the surface. When averaged, the total misfit is similar (<0.07) for FS1 and FS2, less than 3 EDHD, while the total misfit at 10 EDHD is about 15% smaller for FS2 than that for FS1. This is mainly due to a more accurately modeled Rayleigh wave for FS2 than for FS1 (see below).

Figure 4 shows comparisons of the reflectivity solution to the FD-averaged (where applicable) solutions and the differences between the two different free-surface boundary conditions at sites 1 (0.5 EDHD) and 20 (10 EDHD). The averaged seismograms clearly show an improved fit compared to the reflectivity solution.

We estimated the required amount of cpu time to be 10% smaller for FS2 compared to that for FS1. However, it should be noted that this estimate includes differences in the internal FD update near the free surface for the two approaches, in addition to the cost within the free-surface routines.

Conclusions

We have tested the accuracy of two explicit planar free-surface boundary conditions for the 3D fourth-order velocity-stress staggered-grid FD method, implemented 1/2 grid point apart in the vertical direction. The accuracy of the imple-

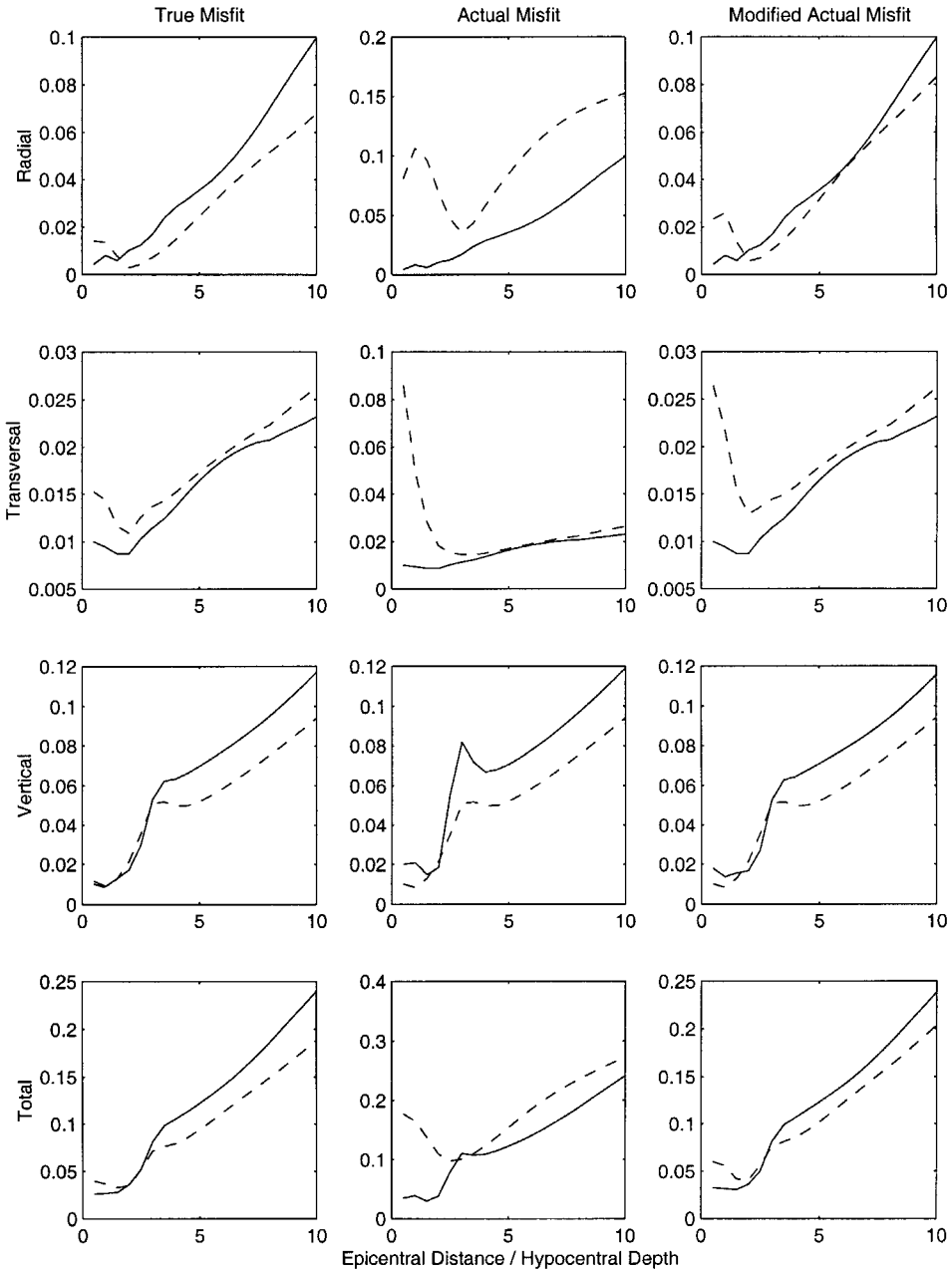

Figure 2. Accuracy of the two implementations of the free-surface boundary condition. Misfit for left column: reflectivity solution at staggered positions (true misfit); middle column: reflectivity solution at the free surface (actual misfit); and right column: reflectivity solution at the free surface and averaged FD results (modified actual misfit). Solid and dashed lines depict the misfit for FS1 and FS2, respectively (see text).

mentations is estimated as the fit between the seismograms from the FD solutions and those computed by a reflectivity method for a uniform half-space model. First, the misfit is estimated using reflectivity solutions at the vertical positions where the FD seismograms are computed, which due to the staggered grid are located 1/2 grid point below the free surface for some components. At 10 EDHD, the misfit is similar and small for the transverse component (<0.03), while the appearance of the Rayleigh wave causes the misfit for the radial and vertical components as well as the total (added for all three components) misfit to be about 22% smaller for FS2 compared to that for FS1.

Then we estimated the misfit using reflectivity solutions at the free surface, namely, a measure including the misfit due to some components positioned 1/2 grid point below the free surface, which is the misfit that is encountered in reality. At 10 EDHD, FS1 (misfit < 0.1) is superior to FS2 (misfit < 0.15) for the horizontal components (located at

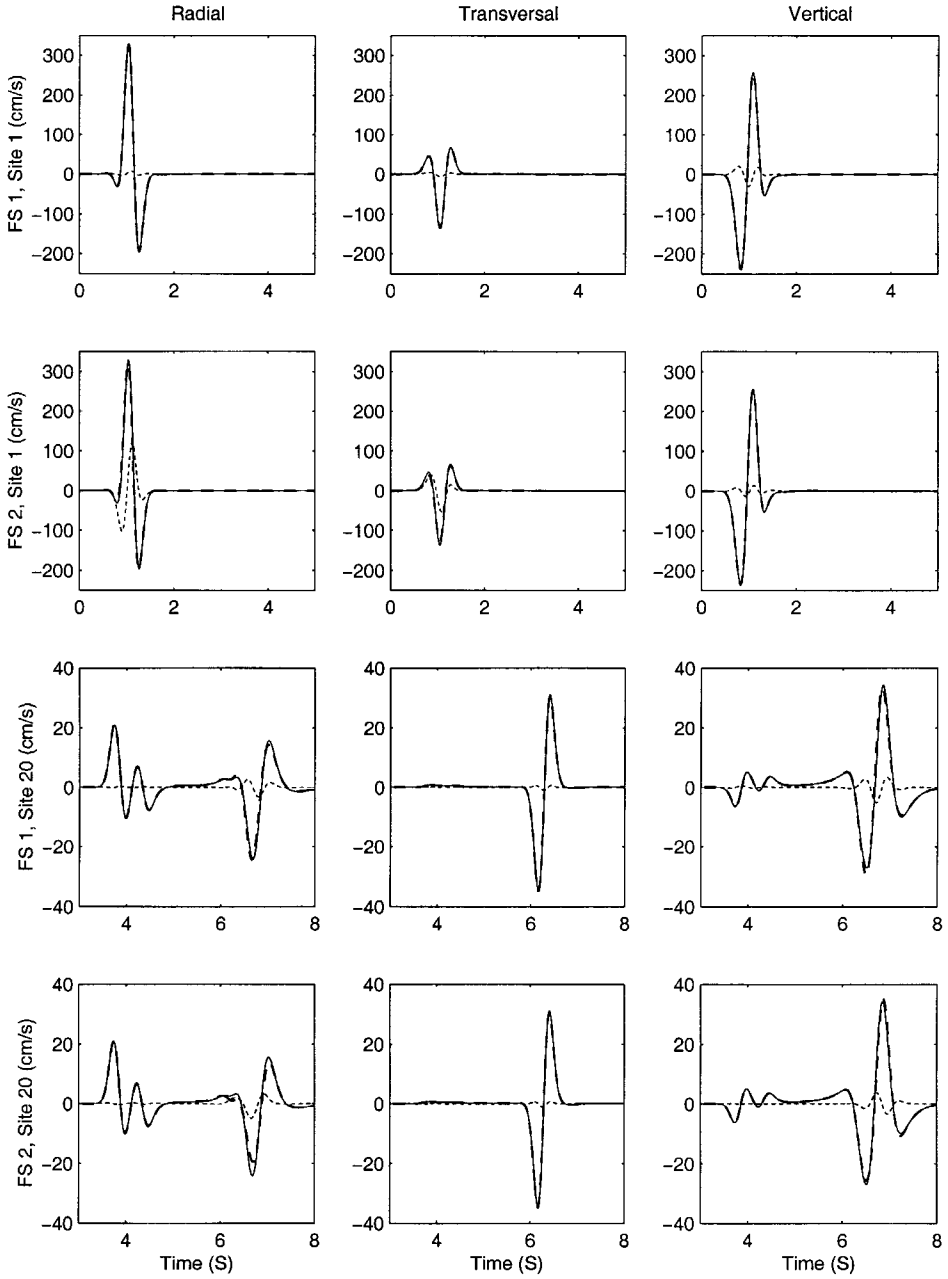

Figure 3. Comparison of surface velocity time histories for the two implementations of the FD free-surface condition discussed in the article (FS1 and FS2, long dashed traces) to the reflectivity solution (solid traces, actual misfit). The short dashed line shows the difference between the reflectivity and FD solutions. The difference is multiplied by 5 for site 1, while the actual difference is shown for site 20.

the surface for FS1, 1/2 grid point below for FS2), while FS2 (misfit 0.093) is more accurate than FS1 (misfit 0.12) for the vertical component (positioned at the surface for FS2, 1/2 grid point below for FS1). In addition, the misfit for FS2 is much larger than that for FS1 close to the epicenter. FS1 is generally more accurate than FS2 when all components are considered.

Finally, we proposed to compute a more accurate estimate of the FD seismograms for the components positioned 1/2 grid point away from the free surface by a simple average between the values immediately above and below the surface. We obtained a misfit up to three times smaller for the averaged seismograms compared to that for the unaveraged seismograms at locations 1/2 grid point below the surface. When averaged, the total misfit is similar (<0.07), less than 3 EDHD, while the misfit is about 15% smaller for FS2 than that for FS1 at 10 EDHD, mainly due to a more accurately modeled Rayleigh wave for FS2. Our recommendation is to

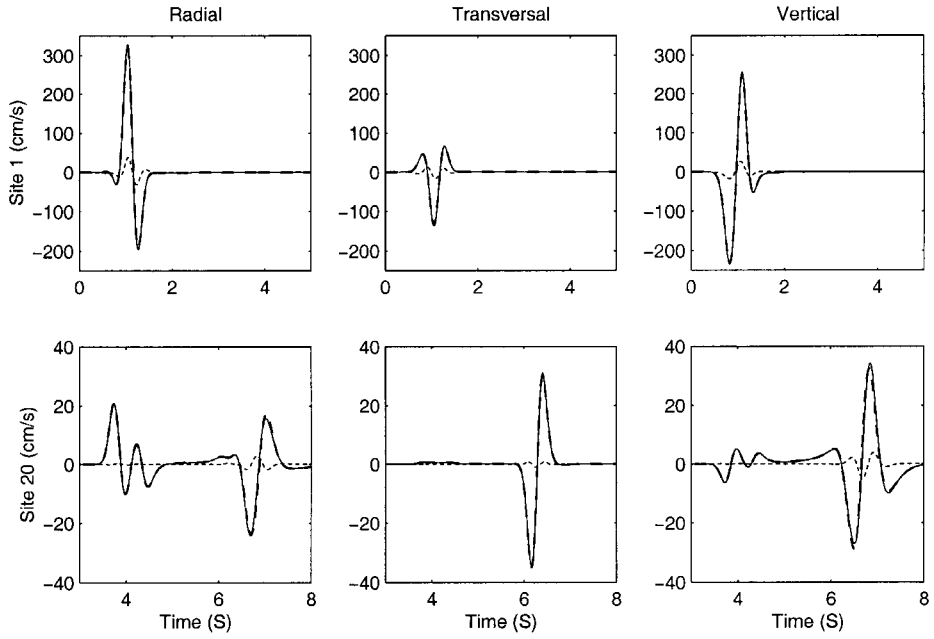

Figure 4. Same as Figure 3, but averaged seismograms are shown when applicable.

use the averaged FS2 that generally produces the most accurate results.

Acknowledgments

We thank Raul Madariaga for helpful advice on the error analysis. We are grateful to Steve Day for advice on the deconvolution procedure in the comparisons. The computations in this study were carried out on the SGI Origin 2000 at MRL, (NSF Grant CDA 96-01954), and Sun Enterprise, ICS, UCSB, with support from NSF Grant EAR 96-28682 and the Southern California Earthquake Center (SCEC), USC 572726 through the NSF cooperative agreement EAR-8920136. This is ICS Contribution Number 376-114EQ and SCEC Contribution Number 555.

References

Bouchon, M. (1981). A simple method to calculate Green's function for layered media, *Bull. Seism. Soc. Am.* **71,** 959–971.

Graves, R. W. (1996). Simulating seismic wave propagation in 3D elastic media using staggered grid finite differences, *Bull. Seism. Soc. Am.* **86,** 1091–1106.

Graves, R. W. (1998). 3D finite difference modeling of the San Andreas fault: source parameterization and ground motion levels, *Bull. Seism. Soc. Am.* **88,** 881–897.

Hestholm, S. O., and B. O. Ruud (1998). 3-D finite-difference elastic wave modeling including surface topography, *Geophysics* **63,** 613–622.

Levander, A. (1988). Fourth-order finite-difference P-SV seismograms, *Geophysics* **53,** 1425–1436.

Ohminato, T., and B. A. Chouet (1997). A free surface boundary condition for including 3D topography in the finite difference method, *Bull. Seism. Soc. Am.* **87,** 494–515.

Olsen, K. B. (1994). Simulation of three-dimensional wave propagation in the Salt Lake Basin, *Ph.D. Thesis,* University of Utah.

Olsen, K. B. (2000). Site amplification in the Los Angeles basin from 3D modeling of ground motion, *Bull. Seism. Soc. Am.* (in press).

Olsen, K. B., and R. J. Archuleta (1996). Three-dimensional simulation of earthquakes on the Los Angeles fault system, *Bull. Seism. Soc. Am.* **86,** 575–596.

Olsen, K. B., R. J. Archuleta, and J. R. Matarese (1995). Three-dimensional simulation of a magnitude 7.75 earthquake on the San Andreas fault, *Science* **270,** 1628–1632.

Olsen, K. B., R. Madariaga, and R. J. Archuleta (1997). Three-dimensional dynamic simulation of the 1992 Landers earthquake, *Science* **278,** 834–838.

Olsen, K. B., R. Nigbor, and T. Konno (2000). 3D viscoelastic wave propagation in the Upper Borrego Valley, California, constrained by borehole and surface data, *Bull. Seism. Soc. Am.* **90,** 134–150.

Peyrat, S., K. B. Olsen, and R. Madariaga (2001). Dynamic modeling of the 1992 Landers earthquake, *J. Geophys. Res.* (in press).

Robertsson, J. O. A. (1996). A numerical free-surface condition for elastic/viscoelastic finite-difference modeling in the presence of topography, *Geophysics* **61,** 1921–1934.

Wald, D., and R. W. Graves (1998). The seismic response of the Los Angeles basin, California, *Bull. Seism. Soc. Am.* **88,** 337–356.

Geophysikalisches Institut
Karlsruhe Universität
76187 Karlsruhe, Germany
(E.G.)

Institute for Crustal Studies
UC Santa Barbara
Santa Barbara, California 93106-1100
(K.B.O.)

Manuscript received 20 September 2000.